A model study of warming-induced phosphorus-oxygen feedbacks in open-ocean oxygen minimum zones on millennial timescales

Daniela Niemeyer[1], Tronje P. Kemena[1], Katrin J. Meissner[2], Andreas Oschlies[1]

[1]Helmholtz-Zentrum für Ozeanforschung Kiel (GEOMAR), Düsternbrooker Weg 20, 24105 Kiel, Germany
5 [2]Climate Change Research Centre and ARC Centre of Excellence for Climate System Science, University of New South Wales, Level 4 Mathews Building, Sydney, New South Wales, 2052, Australia

Correspondence to: D. Niemeyer (dniemeyer@geomar.de)

Abstract. Observations indicate an expansion of oxygen minimum zones (OMZs) over the past 50 years, likely related to ongoing deoxygenation caused by reduced oxygen solubility, changes in stratification and circulation, and a potential
10 acceleration of organic matter turnover in a warming climate. The overall area of ocean sediments that are in direct contact with low oxygen bottom waters also increases with expanding OMZs. This leads to a release of phosphorus from ocean sediments. If anthropogenic carbon dioxide emissions continue unabated, higher temperatures will cause enhanced weathering on land, which, in turn, will increase the phosphorus and alkalinity fluxes into the ocean and therefore raise the ocean's phosphorus inventory even further. A higher availability of phosphorus enhances biological production,
15 remineralisation and oxygen consumption, and might therefore lead to further expansions of OMZs, representing a positive feedback. A negative feedback arises from the enhanced productivity-induced drawdown of carbon and also increased uptake of CO_2 due to weathering-induced alkalinity input. This feedback leads to a decrease in atmospheric CO_2 and weathering rates. Here we quantify these two competing feedbacks on millennial timescales for a high CO_2 emission scenario. Using the UVic Earth System Climate Model of intermediate complexity, our model results suggest that the
20 positive benthic phosphorus release feedback has only a minor impact on the size of OMZs in the next 1000 years. The increase in the marine phosphorus inventory under assumed business-as-usual global warming conditions originates, on millennial timescales, almost exclusively (>80%) from the input via terrestrial weathering and causes a 4 to 5-fold expansion of the suboxic water volume in the model.

1 Introduction

Oxygen minimum zones (OMZs) have more than quadrupled over the past 50 years and it has been suggested that this expansion is related to recent climate change (STRAMMA ET AL., 2008; SCHMIDTKO ET AL., 2017). However, current CO_2 emission-forced models are challenged to reproduce this expansion in detail (STRAMMA ET AL., 2012; CABRE ET AL., 2015).

5 There are at least three different processes that can have an impact on the size of OMZs in a warming climate: ocean warming and its impact on solubility of O_2 in the ocean (BOPP ET AL., 2002), changes in ocean dynamics, e.g. stratification, convective mixing and circulation (MANABE & STOUFFER, 1993; SARMIENTO ET AL., 1998), biological production effects (BOPP ET AL., 2002) including possible CO_2-driven changes in stoichiometry (OSCHLIES ET AL., 2008) and CO_2 induced changes in ballasting particle export (HOFMANN & SCHELLNHUBER, 2010). Here we investigate how changes in biological

10 production and subsequent remineralisation can affect OMZs in addition to the above-mentioned thermal and dynamic effects. We focus on changes in the phosphorus (P) cycle. P is the main limiting nutrient on long timescales (TYRELL, 1999; PALASTANGA ET AL., 2011) and we examine possible effects of changes in the P cycle on millennial timescales.

The major source of P for the ocean is river input (FILIPPELLI, 2008; PAYTON & MCLOUGHLIN, 2007; FÖLLMI, 1996, PALASTANGA ET AL., 2011; FROELICH ET AL., 1982), which is determined by terrestrial weathering of apatite (FILIPPELLI,

15 2002; FÖLLMI, 1996). The main factors controlling terrestrial weathering are temperature, precipitation and vegetation. Higher temperatures are generally associated with enhanced precipitation and in many places with higher terrestrial net primary productivity (MONTEIRO ET AL., 2012), which all tend to increase weathering rates (BERNER, 1991).

It is difficult to determine how much of the globally weathered P enters the ocean in a bioavailable form. Today, about 0.09 - 0.15 Tmol a^{-1} of prehuman, potentially bioavailable P is transported globally by rivers including dissolved organic and

20 inorganic P, particulate organic P and ironbound P (COMPTON ET AL., 2000). About 25% of this potentially bioavailable P is trapped in coastal estuaries and will not enter the open ocean (COMPTON ET AL., 2000). RUTTENBERG (2004) estimated a bioavailable P flux under preindustrial conditions including dissolved P and bioavailable particulate P (=35% of total particulate P) of 0.24-0.29 Tmol P a^{-1} excluding the atmospheric input (RUTTENBERG, 2004). Marine organisms take up P most easily as dissolved inorganic P (DIP). Riverine measurements suggest that only a small fraction of the total P (0.012 to

25 0.032 Tmol a^{-1}) enters the ocean as DIP (FILIPPELLI, 2002; HARRISON ET AL., 2005; COMPTON ET AL., 2000; WALLMANN, 2010; PALASTANGA ET AL., 2011; RUTTENBERG, 2004). However, passing through estuaries can increase the fraction of DIP by 50% (FROELICH, 1984) to 80% (BERNER & RAO, 1994).

After taking up the bioavailable P for photosynthetic production of biomass, a large fraction of the newly produced organic matter is exported out of the euphotic zone as detritus (6.42 Tmol P a^{-1} according to the model study by PALASTANGA ET AL.,

30 2011) and the vast majority of this exported organic matter is remineralised in the deeper ocean by bacteria (6.26 Tmol P a^{-1}; PALASTANGA ET AL., 2011), which is an oxygen consuming process. A small fraction of the exported organic matter is deposited at the sediment surface (0.16 Tmol P a^{-1}; PALASTANGA ET AL., 2011), about 20% of the deposited P is buried in the

sediments on long time scales (0.032 Tmol P a^{-1}; PALASTANGA ET AL., 2011) and the remaining 80% (0.13 Tmol P a^{-1}; PALASTANGA ET AL., 2011) is released back into the water column as DIP, where it is again available for the uptake of marine primary producers (PALASTANGA ET AL., 2011; WALLMANN, 2010).

The processes of burial and release of P are redox-dependent. Under oxic conditions the burial rate is high, while under suboxic conditions the benthic release of P is elevated (INGALL & JAHNKE, 1994; KRAAL ET AL., 2012; WALLMANN, 2010; SLOMP & VAN CAPPELLEN, 2007; FLOEGEL ET AL., 2011; LENTON & WATSON, 2000; TSANDEV & SLOMP, 2009). The redox-dependent release of P into the water column and the decrease in marine oxygen due to remineralisation therefore represent a positive feedback loop on marine biological production (see Fig. 1). Although the feedbacks between ocean and atmosphere are complex (SABINE ET AL., 2004), we assume that an enhanced detritus export into the ocean interior results in an increased marine uptake of atmospheric CO_2 (SARMIENTO & ORR, 1991). Consequently, surface air temperatures decrease with decreasing atmospheric CO_2 concentrations, which, in turn, leads to lower weathering rates (see Fig. 1).

These redox-dependent benthic P fluxes have been investigated in a previous study with the HAMOCC global ocean biogeochemistry model by PALASTANGA ET AL. (2011). PALASTANGA ET AL. (2011) show that doubling the input of dissolved P from rivers results in an increased benthic release of P. This leads to a rise in primary production as well as in oxygen consumption, which in turn affects the oxygen availability in sediments. The benthic release of P acts therefore as a positive feedback on expanding oxygen minimum zones on timescales of 10,000 to 100,000 years (PALASTANGA ET AL., 2011).

Other studies on marine oxygen deficiency focused on the geological past, especially the mid-Cretaceous warm period (120-80 Ma ago) (TSANDEV & SLOMP, 2009; HANDOH & LENTON, 2003; BJERRUM ET AL., 2006; FÖLLMI ET AL., 1996). Several periods of oceanic oxygen depletion have been inferred from sediment data of black shales (SCHLANGER & JENKYNS, 1976), for example for the Cretaceous oceanic anoxic event 2 (OAE) at the Cenomanian-Turonian boundary (93.5 Myrs). Whether processes such as surface warming, sea-level rise (HANDOH & LENTON, 2003), and possibly a slow-down of the ocean overturning circulation and vertical mixing (MONTEIRO ET AL., 2012; TSANDEV & SLOMP, 2009; RUVALCABA BARONI ET AL., 2014) - as assumed for the Cretaceous - will lead to widespread oxygen depletion in the future, is a reason of concern. Consequently, a better understanding of biogeochemical processes associated with Cretaceous OAE might help assess the risk of possible future events of low marine oxygen concentrations (TSANDEV & SLOMP, 2009).

In contrast to previous studies that focus on the geological past, we investigate possible future changes over the next 1000 years using an Earth System Climate Model of intermediate complexity to investigate the feedbacks between the P cycle and OMZs under the extended Representative Concentration Pathways-Scenario 8.5 (RCP 8.5) of the Intergovernmental Panel on Climate Change (IPCC) AR5 report. The RCP 8.5 scenario is characterised by an increase in atmospheric CO_2 concentrations and associated with an increase in radiative forcing of up to 8.5 W m^{-2} by year 2100 (in comparison to preindustrial conditions) and is also known as the "business as usual" scenario (RIAHI ET AL., 2011).

2 Methods

2.1 UVic Model

The University of Victoria Earth System Climate Model (UVic ESCM) version 2.9 (WEAVER ET AL., 2001; EBY ET AL., 2009) is a model of intermediate complexity and consists of a terrestrial model based on TRIFFID and MOSES (MEISSNER ET AL., 2003) including weathering (MEISSNER ET AL., 2012), an atmospheric energy-moisture-balance model (FANNING & WEAVER, 1996), a CaCO$_3$-sediment model (ARCHER, 1996), a sea-ice model (SEMTNER, 1976; HIBLER, 1979; HUNKE & DUKOWICZ, 1997) and a three-dimensional ocean circulation model (MOM2) (PACANOWSKI, 1995). The ocean model includes a marine ecosystem model based on a nutrient-phytoplankton-zooplankton-detritus model (KELLER ET AL., 2012). The horizontal resolution of all model components is 1.8° latitude x 3.6° longitude. The ocean model has 19 layers with layer thicknesses ranging from 50 m at the sea surface to 500 m in the deep ocean. We use a sub-grid scale bathymetry as described in SOMES ET AL. (2013) to simulate benthic fluxes of phosphorus. The sub-grid bathymetry is inferred from the ETOPO2v2[*] and represents global spatial distributions of continental shelves, slopes and other topographical features (1/5°). For the topography used here, the shelf (0-200 m) covers 6.5%, the slope (200-2000 m) 11.7% and the deep sea (>2000 m) 81.9% of the global ocean. Downward fluxes of organic matter are intercepted by the sub-grid bathymetry related to the fractional sediment cover for each ocean grid box, and benthic fluxes of phosphorus are calculated based on the transfer functions described in the following section.

2.2 Phosphorus Cycle in UVic Model

Earlier applications of the UVic ESCM assumed a fixed marine P inventory. We included a representation of the dynamic P cycle for this study. It consists of a modified terrestrial weathering module (MEISSNER ET AL., 2012) and a redox-sensitive transfer-function for burial and benthic release of P (FLOEGEL ET AL., 2011; WALLMANN, 2010).

The continental-weathering module developed earlier for fluxes of dissolved inorganic carbon (DIC) and alkalinity (MEISSNER ET AL., 2012; LENTON & BRITTON, 2006), is based on the following equations:

$$F_{DIC,w} = F_{DIC,w,0} * \lfloor f_{Si} + f_{Ca} * \left(\frac{NPP}{NPP_0}\right) * (1 + 0.087 * (SAT - SAT_0)) \rfloor = F_{DIC,w,0} * f\ (NPP, SAT) \qquad \text{Eq. (1)}$$

$$F_{Alk,w} = F_{Alk,w,0} * \left(\frac{NPP}{NPP_0}\right) * \lfloor f_{Si} * (1 + 0.038) * (SAT - SAT_0) * 0.65^{0.09} * (SAT - SAT_0) \rfloor + f_{Ca} * (1 + 0.087 * (SAT - SAT_0)) \qquad \text{Eq. (2)}$$

---

[*] https://www.ngdc.noaa.gov/mgg/global/etopo2.html

Where $F_{DIC,w}$ and $F_{Alk,w}$ represent the globally integrated flux of DIC and alkalinity via river runoff, f_{Si} and f_{Ca} stand for the fraction of silicate (0.25) and carbonate (0.75) weathering, and *NPP* and *SAT* are the global mean net primary production on land and global mean surface air temperature over land (in degrees Celsius). The index 0 stands for preindustrial values.

We added the following flux to account for P weathering ($F_{DP,w}$) with the same dependencies on globally and annually averaged net primary production (NPP) and surface air temperature (SAT) as those for DIC:

$$F_{DP,w} = F_{DP,0} * f\ (NPP, SAT) \qquad\qquad \text{Eq. (3)}$$

The global river input of dissolved inorganic P (DIP) is the only continental source for P in the model. The global DIP input is distributed over all coastal points of discharge scaled according to their individual volume discharge. The pre-industrial DIP input to the ocean ($F_{DP,0}$) is assumed to be in steady state and in equilibrium with the total globally integrated preindustrial net burial of P (BUR_P):

$$F_{DP,0} = BUR_{P,0} \qquad\qquad \text{Eq. (4)}$$

We use an empirical transfer function for BUR_P and for the benthic release of DIP (BEN_{DIP}) derived from observations across bottom-water oxygen gradients (WALLMANN, 2010; FLÖGEL ET AL., 2011). The release of dissolved inorganic P (BEN_{DIP}) is calculated as follows:

$$BEN_{DIP} = \frac{BEN_{DIC}}{r_{reg}} \qquad\qquad \text{Eq. (5)}$$

Benthic release of dissolved inorganic carbon (BEN_{DIC}) is calculated from an empirical transfer function (Fig. 2 in FLÖGEL ET AL., 2011) to determine BEN_{DIP} fluxes at the ocean bottom. In our model configuration POC is remineralised completely at the ocean bottom and no ocean-to-sediment-fluxes of POC occur, i.e. $BEN_{DIC} = RR_{POC}$, where RR_{POC} denotes the rain rate of particulate organic carbon to the sediment. WALLMANN (2010) calculated r_{reg} by a regression of observational data to bottom-water oxygen concentrations:

$$r_{reg} = \frac{RR_{POC}}{BEN_{DIP}} = Y_F + A * exp\left(\frac{-[O_2]}{r}\right) \qquad\qquad \text{Eq. (6)}$$

The regeneration ratio is calculated by dividing the depth-integrated rate of organic matter degradation in surface sediments (RR_{POC}) by the benthic flux of dissolved inorganic P into the bottom water (BEN_{DIP}). Parameters are defined as $Y_F = 123 \pm$

24, A = -112 ± 24 and r = 32 ± 19 and O_2 is in μmol/l (WALLMANN, 2010). Under oxic conditions r_{reg} is higher than the Redfield ratio (106; REDFIELD ET AL., 1963) and under oxygen-depleted conditions r_{reg} reduces to 10 (WALLMANN, 2010).

The rain rate of POP (RR_{POP}) is calculated by the rain rate of POC (RR_{POC}) divided by the Redfield ratio. As a result BUR_P can be calculated as follows:

$$BUR_P = RR_{POP} - BEN_{DIP} \hspace{8cm} \text{Eq. (7)}$$

The burial of P (BUR_P) in the sediment is equal to the rain rate of particulate organic P (RR_{POP}) minus BEN_{DIP} (FLOEGEL ET AL., 2011). If the benthic release overcomes the rain rate of POP at depths below 1000 m, the burial is set to zero. Following

10   FLOEGEL ET AL. (2011), this condition is not applied to shallower sediments because these deposits receive both marine particles and high fluxes of riverine particulate phosphorus.

2.3 Model Simulations

Two model simulations were performed. Our control simulation, called simulation REF hereafter, includes neither weathering, benthic release, nor burial of P. The global amount of P in the ocean is therefore conserved in this simulation

15   over time. The second simulation, called WB, includes P weathering as well as benthic burial and release of P but excludes additional anthropogenic input. The spin up was performed by computing the burial and benthic release according to Eq. (6). The weathering fluxes were set to a value to compensate the burial rate (Eq. (4)) during the spin up but not thereafter. After a spin-up of 20,000 years under preindustrial boundary conditions, we forced the model with anthropogenic CO_2 concentrations following the RCP 8.5 scenario of the IPCC AR5 assessment (MEINSHAUSEN ET AL., 2011; RIAHI ET AL.,

20   2011). The CO_2 emissions in the UVic ESCM reach 105.6 Pg CO_2 a^{-1} in year 2100. Between years 2100 and 2150 the models are forced with constant CO_2 emissions (105 Pg CO_2 a^{-1}), followed by a linear decline until year 2250 to a level of 11.5 Pg CO_2 a^{-1} and then linearly to zero emissions in year 3005 (see Fig. 2a). Simulated atmospheric CO_2 concentrations peak in year 2250 with 2148.6 ppmv and equal 1835.8 ppmv in year 3005 (see Fig. 2a).

2.4 Simulated preindustrial equilibrium

25   The UVic ESCM has been validated under present day and preindustrial conditions in numerous studies (EBY ET AL., 2009; WEAVER ET AL., 2001). In particular, KELLER ET AL. (2012) recently compared results of its ocean biogeochemical component to observations and previous model formulations. We therefore concentrate our validation on the new model component in this study, the P cycle.

Estimates of preindustrial burial rates vary over a wide range in the literature. The comprehensive review by SLOMP (2011)

30   reported a burial rate of 0.032-0.35 Tmol P a^{-1} for the total ocean while BATURIN (2007) suggests a burial rate of 0.419 Tmol P a^{-1} based on observational data described in detail by WALLMANN (2010). The burial rate diagnosed by the UVic ESCM in

simulation WB for the total ocean under preindustrial boundary conditions (0.38 Tmol P a^{-1}), is within range of these earlier estimates. The burial at the continental margin (0-200 m) accounts for 50-84% of total burial corresponding to 0.016-0.175 Tmol P a^{-1} calculated in SLOMP (2011). RUTTENBERG (2004) estimated a burial rate at continental margins of 0.15-0.22 Tmol P a^{-1}, while the UVic ESCM calculated a burial rate of 0.33 Tmol P a^{-1} for the continental margins in year 1775. The open

5   ocean burial contributes only a minor part to total burial (0.04-0.13 Tmol P a^{-1}; RUTTENBERG, 2004; in the UVic it is 0.046 Tmol P a^{-1}).

To conserve marine P during long model spin ups, the dissolved weathering flux of P under preindustrial conditions is set equal to the diagnosed total burial rate during the spin-up, 0.38 Tmol P a^{-1}. Following the method of calculating the reactive P flux (defined in RUTTENBERG (2004) as the sum of >50% of TDP (=DOP) plus 25-40% of particulate P flux), our result

10   fits well with estimates summarised by SLOMP (2011) ranging from 0.13 Tmol P a^{-1} (natural P flux) to 0.36 Tmol P a^{-1} (modern P flux) and RUTTENBERG (2004) (0.16-0.32 Tmol P a^{-1}).

Global values for benthic release under preindustrial conditions equal 0.78 Tmol P a^{-1} in the UVic ESCM (simulation WB), while RUTTENBERG (2004) described a range from 0.51 Tmol P a^{-1} to 0.84 Tmol P a^{-1} based on pore water measurements (COLMANN & HOLLAND, 2000) for coastal regions. For the deep sea COLMANN & HOLLAND (2000) specified the benthic

15   release value with 0.41 Tmol P a^{-1}. In the UVic ESCM the benthic release for continental margins was calculated as 0.4816 Tmol P a^{-1} and for the open ocean as 0.2951 Tmol P a^{-1}.

3 Results

3.1 Simulated Climate

The global mean atmospheric surface temperature, as simulated by the WB run, increases until year 2835 and peaks at

20   23.1°C, i.e. 9.9°C above pre-industrial levels. Simulation REF shows similar changes in temperature with an increase until year 2855 and a peak at 23.3°C (see Fig. 2a). Both simulations show a slight recovery in temperatures after the peak (REF: 23.2°C; WB: 23.1°C; year 3005). Atmospheric temperatures in the WB-simulation are slightly lower than in the reference simulation, due to slightly lower carbon dioxide concentrations in the atmosphere, caused by increased global ocean alkalinity (REF: 2.498 mol m^{-3}; WB: 2.481 mol m^{-3}; both for year 3005), the enhanced biological pump and a rise in detritus

25   export rate (see Sect. 3.2), and therefore increased marine uptake of atmospheric CO_2. The impact of the negative feedback via enhanced biotically and chemically induced marine uptake of atmospheric CO_2 on surface air temperatures is thus small compared to the CO_2 induced warming in a high-emission scenario.

Given that the response in temperature is similar for both simulations compared to considerable differences in biological productivity (see below), differences in oxygen concentration mainly originate from biogeochemical changes, which will be

30   discussed in Sect. 3.3.

3.2 Phosphorus Dynamics

The weathering rate (see Fig. 3b) and associated flux of P into the ocean via river discharge more than doubles relative to the pre-industrial situation in our WB-simulation and leads to an enhancement in global mean oceanic P concentrations by 27% over 1000 years (see Fig. 2b). At the same time, benthic burial acts as the only P sink in our model (see Fig. S1), mitigating the total increase in marine P. The P concentration remains constant in the control run REF.

The weathering input in the WB-simulation is largest north of 30°N (0.338 Tmol P a^{-1} in year 3005; see Fig. 3a), while south of 30°S (0.138 Tmol P a^{-1}) and in the low latitude Pacific Ocean the input is lowest (0.117 Tmol P a^{-1}). Weathering fluxes into the low latitude Indian and Atlantic Oceans equal 0.187 and 0.267 Tmol P a^{-1}, respectively.

Increasing P concentrations as well as climate warming result in an increase in net primary production in the ocean (ONPP). Globally integrated ONPP ranges between 43.8 Tmol P a^{-1} (REF) and 44.1 Tmol P a^{-1} (WB) under preindustrial conditions and 65 Tmol P a^{-1} (REF) and 116.4 Tmol P a^{-1} (WB) at year 3005 (see Fig. S1). The main areas of ONPP increase are located in the tropical ocean, where higher temperatures favour net primary production in the model (results not shown).

Due to enhanced P inventory and enhanced ONPP, the WB-simulation also has a higher export rate (8.6 Tmol P a^{-1}, computed at 130m depth; see Fig. 2b) when compared to the reference run (5.5 Tmol P a^{-1}) in year 3005. In the REF simulation, the export rate declines until year 2175 (4.8 Tmol P a^{-1}) in response to enhanced stratification, associated declining nutrient supply and stronger nutrient recycling in the upper layers (SCHMITTNER ET AL., 2008; STEINACHER ET AL., 2010; BOPP ET AL., 2013; MOORE ET AL., 2013; YOOL ET AL., 2013; KVALE ET AL., 2015). The export rate recovers to reach 5.5 Tmol P a^{-1} at the end of the simulation in experiment REF.

The globally integrated remineralisation rate in the aphotic zone (results not shown) ranges between 5.1 Tmol P a^{-1} (WB) and 5.2 Tmol P a^{-1} (REF) in year 1775. Simulation WB is characterized by a strong increase in remineralisation until 3005 with a maximum of 8.1 Tmol P a^{-1} (in year 3005), while in the reference run the remineralisation rate first decreases, followed by a moderate increase to 5.3 Tmol P a^{-1}. Regions with highest remineralisation are located on the continental margins, especially in the Indian Ocean.

The P burial in the WB-simulation equals 0.38 Tmol P a^{-1} in year 1775 and decreases by 44.3% to 0.2 Tmol P a^{-1} in year 3005 (see Fig. S1). One reason for this decrease is the redox-state of the bottom water. The strong expansion of the area of ocean bottom waters with O_2 concentrations below 0.005 mol m^{-3} (see Fig. 2d) in the WB simulation leads to a decrease in benthic burial of P despite an increase in the rain rate of particulate organic P, RR_{POP}. In general, burial rates are largest along the coastal margins, where 87.9% of the total flux is buried in 1775. Highest increases in burial rates between years 1775 and 3005 are located in the Arctic Ocean (see Fig. 4a), whereas burial rates decrease in the Bay of Bengal and the Gulf of Mexico where low-oxygen bottom waters expand (see Fig. 5).

The benthic P release in the WB simulation increases by 119% until year 3005 to 1.7 Tmol P a^{-1} (see Fig. S1). As mentioned above, the benthic release is a redox-dependent process, which commonly takes place at the coastal margins (WALLMANN, 2010; in our model under preindustrial conditions 62% of total release is from coastal margins). This means that an increase

in suboxic bottom water area (see Fig. 2d) leads to an enhanced release of benthic P in WB. A rapid increase between years 1775 and 3005 can be found in the Bay of Bengal, the Gulf of Mexico and in the Arctic Ocean (see Fig. 4b).

In our model simulations, both the weathering-induced P flux into the ocean (see Fig. 2c) as well as the net P released from the sediments (see Fig. 2c) show a strong increase under continued global warming, which explains the increase in the marine P inventory in the WB simulation (see Fig. 2b). However, the simulated increase in the weathering input has a much stronger (about 4 times larger) impact on the P budget and therefore on the expansion of OMZs than the benthic release feedback (see Fig. 2c). We note that even at the end of the thousand-year simulation, the P cycle has not yet reached a new steady state in experiment WB. Weathering rates are high in the warm climate and burial of P has not increased to counteract the supply by weathering (see Fig. 3b & S1). The release of P from sediments also adds to this imbalance. As a result, the marine P inventory is still increasing almost linearly at the end of our simulation. Extending the simulation until year 10,000 reveals that the ocean - as well as the coastal regions - do not become anoxic despite a more than 3-fold increase in oceanic P inventory (see Sect. 3.3 & Supplement Fig. S 2) while the P cycle still exhibits a strong imbalance between sources and sinks.

3.3 Oxygen Response

The black contours in Fig. 5 indicate the lateral extent of OMZs for a depth of 300 m (see Fig. S3 for a depth of 900 m). In year 1775, the suboxic volume, defined here as waters with oxygen concentrations of less than 5 mmol m^{-3}, equals $3.9x10^6$ km^3 in both simulations (see Fig. 2d). An observational estimate of today's suboxic water volume equals $102x10^6 \pm 15x10^6$ km^3 for oxygen concentrations less than 20 mmol m^{-3} (PAULMIER & RUIZ-PINO, 2009), which is considerably larger than the volume of $O_2<20$ mmol m^{-3} waters in our WB-simulation ($WB_{2005} = 15.8x10^6$ km^3). However, in consideration of the studies of BIANCHI ET AL. (2012) and their calculated OMZ volume of $2.28-2.78*10^6$ km^3, as well as World Ocean Atlas ($WOA_{2005} = 4.12*10^5$ km^3), it can be concluded that estimations of the volume of OMZs vary over a wide range and that our results are within this range. Comparing our results with observational data from the WOA, a generally good agreement can be found with regard to the spatial distribution of low-oxygen waters (see Fig. 5). The suboxic areas are located in the upwelling regions of the tropical eastern Pacific and eastern Atlantic as well as in the Indian Ocean (see Fig. 5; representative for both simulations in 1775).

During our transient simulations, we find a considerable expansion of OMZs until year 3005 in both simulations (see Fig. 2d and Fig. 5). The expansion of the suboxic volume between 300 and 900 m is particularly pronounced in the WB simulation where the OMZs account for $4.85x10^7$ km^3 in year 3005, i.e. an increase by a factor 12.4. The control simulation (REF) shows a much smaller increase in the volume of OMZs ($1.12 x 10^7$ km^3 between 300 and 900 m depth). As both simulations display similar climates (see Fig. 2a), the difference in the oxygen fields is largely due to the differences in the simulated P cycle.

The sea-floor area in contact with suboxic bottom waters, which directly impacts the redox-sensitive benthic burial and P release, shows an increase by more than a factor of 19 ($WB_{1775}=3.59x10^5$ km^2; $WB_{3005}=6.95x10^6$ km^2) in the WB simulation

(see Fig. 2d) compared to a factor of 4 increase in the REF simulation (REF$_{1775}$=2.79x10^5 km^2; REF$_{3005}$=1.2x10^6 km^2). Our present-day results (WB$_{2005}$ = 3.8*10^5 km^2) compare well with data of the WOA (WOA$_{2005}$ = 2.48*10^5 km^2).

Somewhat unexpectedly, in our study an increase in continental weathering does not result in an anoxic ocean under current topography and seawater chemistry - at least not until year 10,000. At the preindustrial state (year 1775), 0.12% of all coastal
5 margins are characterized by oxygen concentrations below 0.005 mol m^{-3}. While this portion increases by about a factor of 50 to 5.57% by year 3005, this is too low for the generation of widespread coastal anoxia. Conversely, the global mean oxygen concentration starts to increase again in year 3415 when it has reached a minimum of about two thirds of the pre-industrial oxygen inventory in the WB simulation (see Fig. S1). This suggests that the positive feedback between the release of benthic P and marine net primary production is - in this study for present day bathymetry and geography - not the decisive
10 factor for a rapid transition into an anoxic ocean.

4 Uncertainties

Although the model's subcomponents for weathering, burial and benthic release rates are highly simplified in this study, the simulated global P fluxes fall within the range suggested by earlier studies and observational estimates (PALASTANGA ET AL., 2011; FILIPPELLI, 2002; BATURIN, 2007; WALLMANN, 2010). The weathering fluxes are calibrated against global mean burial
15 rates under an implicit steady-state assumption, although it is unclear whether the pre-industrial P cycle in the ocean was in equilibrium (WALLMANN, 2010). The relatively high P weathering fluxes as well as the assumed indefinite P reservoir in the shelf sediments in our simulations might lead to an overestimation of the effects on the P cycle and OMZs.

In our model, the increase in the P inventory results in a strong increase in ONPP. Contrary to other studies, e.g. GREGG ET AL. (2005) or BOYCE ET AL. (2010), in our study the temperature effect overcompensates the stratification effect as described
20 by SARMIENTO ET AL. (2004), TAUCHER & OSCHLIES (2011) and KVALE ET AL. (2015) and thus leads to an increase in ONPP also in the reference run. While the net effect of warming on ONPP is not well constrained and differs considerably among models, the impact of changing environmental conditions on export production appears to be better constrained (TAUCHER & OSCHLIES, 2011). In agreement with simulations by other models, experiment REF shows a stratification-induced decline in export production, while the increase in P induces an increase in export production in WB. Although we use a coarse
25 resolution model, the applied sub-grid scale bathymetry allows the calculation of more accurate benthic burial and release fluxes than otherwise possible with such a model. It should also be noted that the benthic release feedback on OMZs might have been more efficient under Cretaceous boundary conditions because the shelf area was considerably larger due to higher sea levels (late Cretaceous shelf area: 46x10^6 km^2; present day shelf area: 26x10^6 km^2 (BJERRUM ET AL., 2006)). Cretaceous topography might therefore have induced a stronger benthic release feedback as shown in TSANDEV & SLOMP (2009).
30 FILIPPELLI (2002) showed in his study that due to the anthropogenic activities the global, total present-day river input of P has doubled in the last 150 years. In our study the direct anthropogenic influence, such as agricultural input of P into the system, is excluded and should be considered in future studies even though the human impact is projected to decrease until

year 3500 (FILIPPELLI, 2008). FILIPPELLI (2008) and HARRISON ET AL. (2005) estimated a rate of 0.03 Tmol P a^{-1} and 0.7 Tg P a^{-1} (=0.023 Tmol P a^{-1}), respectively, for anthropogenic P delivered to the ocean as a result of fertilization, deforestation and soil loss as well as sewage in year 3000. In comparison to our simulated maximum weathering value of 1.09 Tmol P a^{-1} until year 3005, the direct anthropogenic impact seems to be small.

5   ## 5 Conclusions

This study constitutes a first approach to estimate the potential impact of changes in the marine P cycle on the expansion of global ocean OMZs under global warming on millennial time scales. Model simulations show that the warming-induced increase in terrestrial weathering (see Fig. 3b) leads to an increase in marine P inventory (see Fig. 2b) resulting in an intensification of the biological pump, corroborating the findings by TSANDEV & SLOMP (2009). As a consequence, oxygen
10   consumption as well as the volume of OMZs increase in our simulations by a factor of 12 over the next millennium (see Fig 2d and 5).

The positive feedback involving redox-sensitive benthic P fluxes - where the expansion of OMZs leads to an increase in benthic release of P (see Fig. 2c and Fig. S1), which in turn enhances biological production and subsequent oxygen consumption (WALLMANN 2010) - has only limited relevance for the expansion of OMZs in this study. Instead, a negative
15   feedback dominates that involves enhanced weathering and P supply to the ocean, an intensification of the biological carbon pump and associated marine uptake of atmospheric CO_2. The atmospheric CO_2 impacts the surface air temperature through a negative feedback loop, which limits the warming and weathering and, eventually, the expansion of the OMZs. We can therefore conclude that, based on the parameterizations used in this study, the P weathering and biological pump feedback outcompetes the redox-sensitive benthic P-release feedback on millennial timescales. Although the ocean does not become
20   anoxic in our simulations, the benthic P-release feedback may have played a role in past oceanic anoxic events. An increase in shelf areas due to higher sea levels, such as during the Cretaceous, would have led to a more powerful benthic P-release feedback as a much larger sediment area could have been in contact with low-oxygen bottom waters. Whether this different bathymetry alone could result in a more dominant benthic P-release feedback needs to be investigated in future studies.

Acknowledgments

25   The model data will be available at http://data.geomar.de/thredds/catalog/open_access/niemeyer-et-al_2016/catalog.html. This work is a contribution to the Sonderforschungsbereich (SFB) 754 "Climate-Biogeochemical Interactions in the Tropical Ocean" and the BMBF project PalMod. We thank M. Eby for his excellent help with the UVic ESCM and K. F. Kvale and J. Getzlaff for proofreading. KJM is thankful for UNSW Science Silver- and Goldstar Awards.

30

References

ARCHER, D.: A data-driven model of the global calcite lysocline. Glob. Biogeochem. Cycles, 10 (3), 511-526, doi: 10.1029/96GB01521, 1996.

BATURIN, G. N.: Issue of the Relationship between Primary Productivity of Organic Carbon in Ocean and Phosphate Accumulation (Holocene-Late Jurassic). Lith. Mineral Res., 42, 318-348, doi: 10.1134/S0024490207040025, 2007.

BERNER, R. A.: Weathering, plants and the long-term carbon cycle. Geochim. Cosmochim. Acta, 56, 3225-3231, 1991.

BERNER, R. A.; RAO, J.-L.: Phosphorus in sediments of the Amazon River and estuary: Implications for the global flux of phosphorus to the sea. Geochim. Cosmochim. Acta, 58 (10), 2333-2339, 1994.

BIANCHI, D.; DUNNE, J. P.; SARMIENTO, J. L.; GALBRAITH, E. D.: Data-based estimates of suboxia, denitrification, and N2O production in the ocean and their sensitivities to dissolved O2. Glob. Biogeochem. Cycles, 26, doi: 10.1029/2011GB004209, 2012.

BJERRUM, C. J.; BENDTSEN, J.; LEGARTH, J. I. F.: Modelling organic carbon burial during sea level rise with reference to the Cretaceous. Geochem. Geophys., 7 (5), doi: 10.1029/2005GC001032, 2006.

BOPP, L.; LE QUERE, C.; HEIMANN, M.; MANNING, A.: Climate-induced oceanic oxygen fluxes: Implications for the contemporary carbon budget. Glob. Biogeochem. Cycles, 16 (2), 6-1 - 6-13, doi: 10.1029/2001GB001445, 2002.

BOPP, L.; RESPLANDY, L.; ORR, J. C.; DONEY, S. C.; DUNNE, J. P.; GEHLEN, M.; HALLORAN, P.; HEINZE, C.; ILLYINA, T.; SEFERIAN, R.; TJIPUTRA, J.; VOICHI, M.: Multiple stressors of ocean ecosystems in the 21st century: projections with CMIP5 models. Biogeosciences, 10, 6225-6245, doi: 10.5194/bg-10-6225-2013, 2013.

BOYCE, D. G.; LEWIS, M. R.; WORM, B.: Global phytoplankton decline over the past century. Nature, 466, 7306, 591-596, 2010.

CABRÉ, A.; MARINOV, I.; BERNARDELLO, R.; BIANCHI, D.: Oxygen minimum zones in the tropical Pacific across CMIP5 models: mean state differences and climate change trends. Biogeosciences, 12, 5429-5454, 2015.

COLMANN, A. S.; HOLLAND, H. D.: The global diagenetic flux of phosphorus from marine sediments to the ocean: Redox sensitivity and the control of atmospheric oxygen levels. Marine Authigenesis: from global to Microbial, 66, 53-75, 2000.

COMPTON, J.; MALLINSON, D.; GLENN, C. R.; FILIPPELLI, G.; FÖLLMI, K.; SHIELDS, G.; ZANIN, Y.: Variations in the global phosphorus cycle. Marine Authigenesis: From Global to Microbial, 66, 21-33, 2000.

EBY, M.; ZICKFELD, K.; MONTENEGRO, A.; ARCHER, D.; MEISSNER, K. J.; WEAVER, A. J.: Lifetime of Anthropogenic Climate Change: Millennial Time Scales of Potential CO_2 and Surface Temperature Perturbations. J. Climate, 22, 2501-2511, doi: 10.1175/2008JCLI2554.1, 2009.

FANNING, A.G.; WEAVER, A. J.: An atmospheric energy-moisture model: Climatology, interpentadal climate change and coupling to an ocean general circulation model. J. Geophys. Res., 101, 15111–15128, doi: 10.1029/96JD01017, 1996.

FILIPPELLI, G. M.: The Global Phosphorus Cycle. Rev. Mineral. Geochem., 48, 391-425, doi: 10.2138/rmg.2002.48.1, 2002.

FILIPPELLI, G. M.: The Global Phosphorus Cycle: Past, Present, and Future. Elements, 4 (2), 89-95, doi: 10.2113/GSELEMENTS.4, 2008.

FLOEGEL, S.; WALLMANN, K.; POULSON, C. J.; ZHOU, J.; OSCHLIES, A.; VOIGT, S.; KUHNT, W.: Simulating the biogeochemical effects of volcanic CO_2 degassing on the oxygen-state of the deep ocean during the Cenomanian/Turonian Anoxic Event (OAE2). Earth. Planet. Sci. Lett., 305, 371-384, doi: 10.1016/j.epsl.2011.03.018, 2011.

FÖLLMI, K. B.: The phosphorus cycle, phosphogenesis and marine phosphate-rich deposits. Earth-Sci. Rev., 40, 55-124, doi: 10.1016/0012-825200049-6, 1996.

FROELICH, P. N.; BENDER, M. L.; LUEDTKE, N. A.: The marine phosphorus cycle. Am. J. of Sci., 282, 474-511, doi: 10.2475/ajs.282.4.474, 1982.

FROELICH P. N.: Interactions of the marine phosphorus and carbon cycles, in Moore, B. and Dastoor, M. N., eds., The Interaction of Global Biogeochemical Cycles: Pasadena, California Institute of Technology, NASA - JPL Publication 84-21, 141-176, 1984.

GREGG, W. G.; CASEY, N. W.; MCCLAIN, C. R.: Recent trends in global ocean chlorophyll. Geophys. Res. Lett., 32, doi: 10.1029/2004GL021808, 2005.

HANDOH, I.; LENTON, T. M.: Periodic mid-Cretaceous oceanic anoxic events linked by oscillations of the phosphorus and oxygen biogeochemical cycles. Glob. Biogeochem. Cycles, 17 (4), doi: 10.1029/2003GB002039, 2003.

HARRISON J.; SEITZINGER S. P.; BOUWMAN F.; CARACO N. F.; BEUSEN A. H. W.; VÖRÖSMARTY C. J.: Dissolved inorganic phosphorus export to the coastal zone: Results from a spatially explicit, global model. Glob. Biogeochem. Cycles, 19 (4), doi: 10.1029/2004GB002357, 2005.

HIBLER, W. D.: A dynamic thermodynamic sea ice model. J. Phys. Oceanogr., 9, 815–846, 1979.

HOFMANN, M.; SCHELLNHUBER, H. J.: Ocean acidification: a millennial challenge. Energy Environ. Sci., 3, 1883-1896, doi: 10.1039/C000820F, 2010.

HUNKE, E. C.; DUKOWICZ, J. K.: An Elastic-Viscous-Plastic Model for Sea Ice Dynamics. J. Phys. Oceanogr., 27 (9), 1849-1867, 1997.

INGALL, E.: JAHNKE, R.: Evidence for enhanced phosphorus regeneration from marine sediments overlain by oxygen depleted waters. Geochim. Cosmochim. Acta, 58 (11), 2571-2575, doi: 10.1016/0016-7037(94)90033-7, 1994.

KELLER, D. P.; OSCHLIES, A.; EBY, M.: A new marine ecosystem model for the University of Victoria Earth System Climate Model. Geosci. Model Dev., 5, 1195-1220, doi: 10.5194/gmd-5-1195-2012, 2012.

KRAAL, P.; SLOMP, C. P.; REED, D. C.; REICHART, G.-J.; POULTON, S. W.: Sedimentary phosphorus and iron cycling in and below the oxygen minimum zone of the northern Arabian Sea. Biogeosciences, 9, 2603-2624, doi: 10.5194/bg-9-2603-2012, 2012.

KVALE, K. F.; MEISSNER, K. J.; KELLER, D. P.: Potential increasing dominance of heterotrophy in the global ocean. Env. Res. Let., 10, 7, doi: 10.1088/1748-9326/10/7/074009, 2015.

LENTON, T. M.; BRITTON, C.: Enhanced carbonate and silicate weathering accelerates recovery from fossil fuel CO_2 perturbations. Glob. Biogeochem. Cycles, 20, doi: 10.1029/2005GB002678, 2006.

LENTON, T. M.; WATSON, A. J.: Redfield revisited. 1. Regulation of nitrate, phosphate, and oxygen in the ocean. Glob. Biogeochem. Cycles, 14 (1), 225-248, doi: 10.1029/1999GB900065, 2000.

MANABE, S.; STOUFFER, R. J.: Multiple-Century Response of a Coupled Ocean-Atmosphere Model to an increase of Atmospheric Carbon Dioxide. J. Climate 7, 5-23, 1993.

MEINSHAUSEN, M.; SMITH, S. J.; CALVIN, K.; DANIEL, J. S.; KAINUMA, M. L. T.; LAMARQUE, J.-F.; MATSUMOTO, K.; MONTZKA, S. A.; RAPER, S. C. B.; RIAHI, K.; THOMSON, A.; VELDERS, G. J. M.; VAN VUUREN, D. P. P.: The RCP greenhouse gas concentrations and their extensions from 1765 to 2300. Climatic Change, 109, 213-241, doi: 10.1007/s10584-011-0156-z, 2011.

MEISSNER, K. J.; MCNEIL, B.; EBY, M.; WIEBE, E. C.: The importance of the terrestrial weathering feedback for multimillenial coral reef habitat recovery. Glob. Biogeochem. Cycles, 26, doi: 10.1029/2011GB004098, 2012.

MEISSNER, K. J.; WEAVER, A. J.; MATTHEWS, H. D.; COX, P. M.: The role of land surface dynamics in glacial inception: a study with the UVic Earth System Model. Clim. Dynam., 21, 515-537, doi: 10.1007/s00382-003-0352-2, 2003.

MONTEIRO, F. M.; PANCOST, R. D.; RIDGWELL, A.; DONNADIEU, Y.: Nutrients as the dominant control on the spread of anoxia and euxinia across the Cenomanian-Turonian oceanic anoxic event (OAE2): Model-data comparison. Paleoceanogr., 27, doi: :10.1029/2012PA002351, 2012.

MOORE, J. K.; LINDSAY, K.; DONEY, S. C.; LONG, M. C.; MISUMI, K.: Marine Ecosystem Dynamics and Biogeochemical Cycling in the Community Earth System Model [CESM1(BGC)]: Comparison of the 1990s with the 2090s under the RCP4.5 and RCP8.5 Scenarios. J. Clim., 26, 9291-9312, doi: 10.1175/JCLI-D-12-00566.1, 2013.

OSCHLIES, A.; SCHULZ, K. G.; RIEBESELL, U.; SCHMITTNER, A.: Simulated 21st century's increase in oceanic suboxia by CO_2-enhanced biological carbon export, Global Biogeochem. Cycles, 22, doi: 10.1029/2007GB003147, 2008.

PACANOWSKI, R.C.: MOM 2 Documentation User's Guide and Reference Manual, Version 1.0. GFDL Technical Report, 1995.

PALASTANGA, V.; SLOMP, C. P.; HEINZE, C.: Long-term controls on ocean phosphorus and oxygen in a global biogeochemical model. Glob. Biogeochem. Cycles 25, doi: 10.1029/2010GB003827, 2011.

PAULMIER, A.; RUIZ-PINO, D.: Oxygen minimum zones (OMZs) in the modern ocean. Prog. Oceanogr., 80, doi: 10.1016/j.pocean.2008.08.001, 2009.

PAYTON, A.; MCLOUGHLIN, K.: The Oceanic Phosphorus Cycle. Chem. Rev., 107, 563-576, doi: 10.1021/cr0503613, 2007.

REDFIELD, A.C.; KETCHUM, B.H.; RICHARDS, F.A.: The influence of organisms on the composition of seawater. The Sea. Ed. M.N. Hill, 2, 26-77, 1963.

RIAHI, K.; RAO, S.; KREY, V.; CHO, C.; CHIRKOV, V.; FISCHER, G.; KINDERMANN, G.; NAKICENOVIC, N.; RAFAJ, P.: RCP 8.5 – A scenario of comparatively high greenhouse gas emissions. Clim. Chang., 109, 33-57, doi: 10.1007/s10584-011-0149-y, 2011.

RUTTENBERG, K. C.: The global phosphorus cycle. The Global Phosphorus Cycle. Treatise on Geochemistry, edited by W. Schlesinger, pp. 585-643, Elsevier, Amsterdam, 2004.

RUVALCABA BARONI, I.; TOPPER, R. P. M.; VAN HELMOND, N. A. G. M.; BRINKHUIS, H.; SLOMP, C. P.: Biogeochemistry of the North Atlantic during oceanic anoxic event 2: roles of changes in ocean circulation and phosphorus input. Biogeosciences, 11, 977-993, doi: 10.5194/bg-11-977-2014, 2014.

SABINE, C. L.; FEELY, R. A.; GRUBER, N.; KEY, R. M.; LEE, K.; BULLISTER, J. L.; WANNINKHOF, R.; WONG, C. S.; WALLACE, D. W. R.; TILBROOK, B.; MILLERO, F. J.; PENG, T.-H.; KOZYR, A.; ONO, T.; RIOS, A. F.: The Oceanic Sink for Anthropogenic CO2. Science, 305, 5682, 367-371, doi: 10.1126/science.1097403, 2004.

SARMIENTO, J. L.; ORR, J. C.: Three-dimensional simulations of the impact of Southern Ocean nutrient depletion on atmospheric CO2 and ocean chemistry. Limnol. Oceanog., 36, 8, 1928-1950, 1991.

SARMIENTO, J. L.; HUGHES, T. M. C.; STOUFFER, R. J.; MANABE, S.: Simulated response of the ocean carbon cycle to anthropogenic climate warming. Letters to Nature, 393, 245-249, doi: 10.1038/30455, 1998.

SARMIENTO, J. L. SLATER, R.; BARBER, R.; BOPP, L.; DONEY, S. C.; HIRST, A. C.; KLEYPAS, J.; MATAER, R.; MIKOLAJEWICZ, U.; MONFRAY, P.; SOLDATOV, V.; SPALL, S. A.; STOUFFER, R.: Response of ocean ecosystems to climate warming. Global Biogeochem. Cycles, 18, doi: 10.1029/ 2003GB002134, 2004.

SCHLANGER, S. O.; JENKYNS, H. C.: Cretaceous oceanic anoxic events: causes and consequences. Geologie en Mijnbouw, 55 (3-4), 1976.

SCHMIDTKO, S.; STRAMMA, L.; VISBECK, M.: Decline in global oceanic oxygen content during the past five decades. Nature, 542, 335-339, doi: 10.1038/nature21399, 2017.

SCHMITTNER, A.; OSCHLIES, A.; MATTHEWS, H. D.; GALBRAITH, E. D.: Future changes in climate, ocean circulation, ecosystems, and biogeochemical cycling simulated for a business-as-usual CO_2 emission scenario until year 4000 AD. Glob. Biogeochem. Cycles, 22, doi: 10.1029/2007GB002953, 2008.

SEMTNER, A. J.: A Model for the Thermodynamic Growth of Sea Ice in Numerical Investigations of Climate. J. Phys. Oceanogr., 6, 379-389, 1976.

SLOMP, C. P.; VAN CAPPELLEN, P.: The global marine phosphorus cycle: sensitivity to oceanic circulation. Biogeosciences, 4, 155-171, doi: 10.5194/bg-4-155-2007, 2007.

SLOMP, C. P.: Phosphorus cycling in the estuarine and coastal zones: Sources, sinks, and transformations. Treatise on Estuarine and Coastal Science, edited by E. Wolanski and D. McLusky, pp. 201, 2011.

SOMES, C. J.; OSCHLIES, A.; SCHMITTNER, A.: Isotopic constraints on the pre-industrial oceanic nitrogen budget. Biogeosciences, 10, doi: 10.5194/bg-10-5889-2013, 2013.

STEINACHER, M.; JOOS, F.; FRÖLICHER, T. L.; BOPP, L.; CADULE, P.; COCCO, V.; DONEY, S. C.; GEHLEN, M.; LINDSAY, K.; MOORE, J. K.; SCHNEIDER, B.; SEGSCHNEIDER, J.: Projected 21st century decrease in marine productivity: a multi-model analysis. Biogeosciences, 7, 979-1005, 2010.

STRAMMA, L.; JOHNSON, G. C.; SPRINTALL, J.; MOHRHOLZ, V.: Expanding Oxygen-Minimum Zones in the Tropical Ocean. Science, 320, 655-658, doi: 10.1126/science.1153847, 2008.

STRAMMA, L.; OSCHLIES, A.; SCHMIDTKO, S.: Mismatch between observed and modelled trends in dissolved upper-ocean oxygen over the last 50 yr. Biogeosciences, 9, 4045-4057, doi: 10.5194/bg-9-4045-2012, 2012.

TAUCHER, J.; OSCHLIES, A.: Can we predict the direction of marine primary production change under global warming? Geophys. Res. Lett, 38, doi: 10.1029/2010GL045934, 2011.

TSANDEV, I. V.; SLOMP, C. P.: Modelling phosphorus cycling and carbon burial during Cretaceous Oceanic Anoxic Events. Earth Planet. Sci. Lett., 286, 71-79, doi: 10.1016/j.epsl.2009.06.016, 2009.

TYRELL, T.: The relative influences of nitrogen and phosphorus on oceanic primary production. Nature, 400, doi: 10.1038/22941, 1999.

WALLMANN, K.: Phosphorus imbalance in the global ocean?. Glob. Biogeochem. Cycles, 24, doi: 10.1029/2009GB003643, 2010.

WEAVER, A. J.; EBY, M.; WIEBE, E. C.; BITZ, C. M.; DUFFY, P. B.; EWEN, T. L.; FANNING, A. F.; HOLLAND, M. M.; MACFADYEN, A.; MATTHEWS, H. D.; MEISSNER, K. J.; SAENKO, O.; SCHMITTNER, A.; WANG, H.; YOSHIMORI, M.: The UVic Earth System Climate Model: Model Description, Climatology and Applications to Past, Present and Future Climates. Atmosphere-Ocean, 39, 4, 361-428, doi: 10.1080/07055900.2001.9649686, 2001.

YOOL, A.; POPOVA, E. E.; COWARD, A. C.; BERNIE, D.; ANDERSON, T. R.: Climate change and ocean acidification impacts on lower trophic levels and the export of organic carbon to the deep ocean. Biogeosciences, 10, 5831-5854, doi: 10.5194/bg-10-5831-2013, 2013.
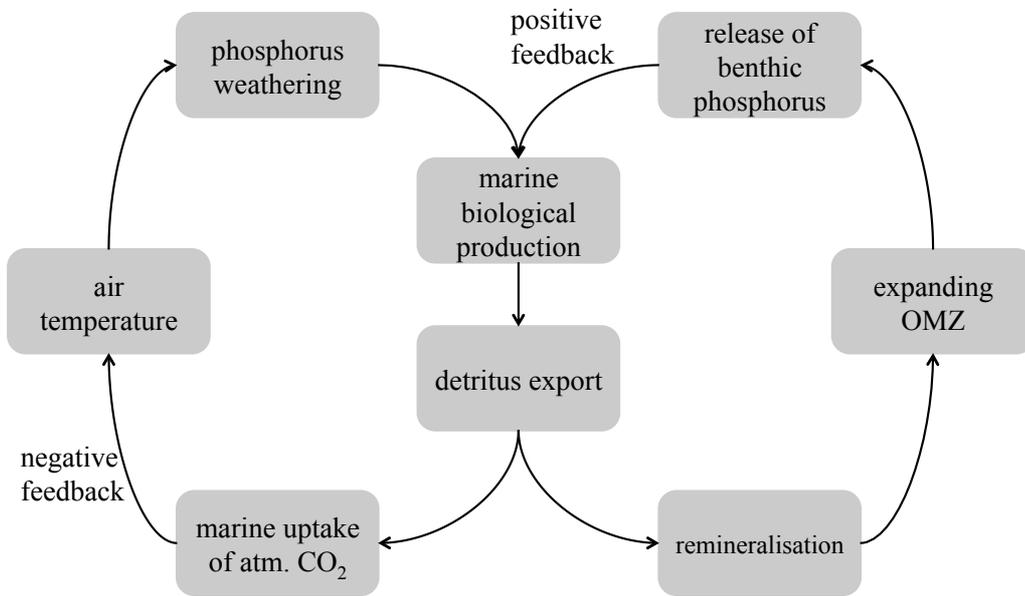
Figure 1: Possible feedbacks in the global phosphorus cycle under climate warming conditions.
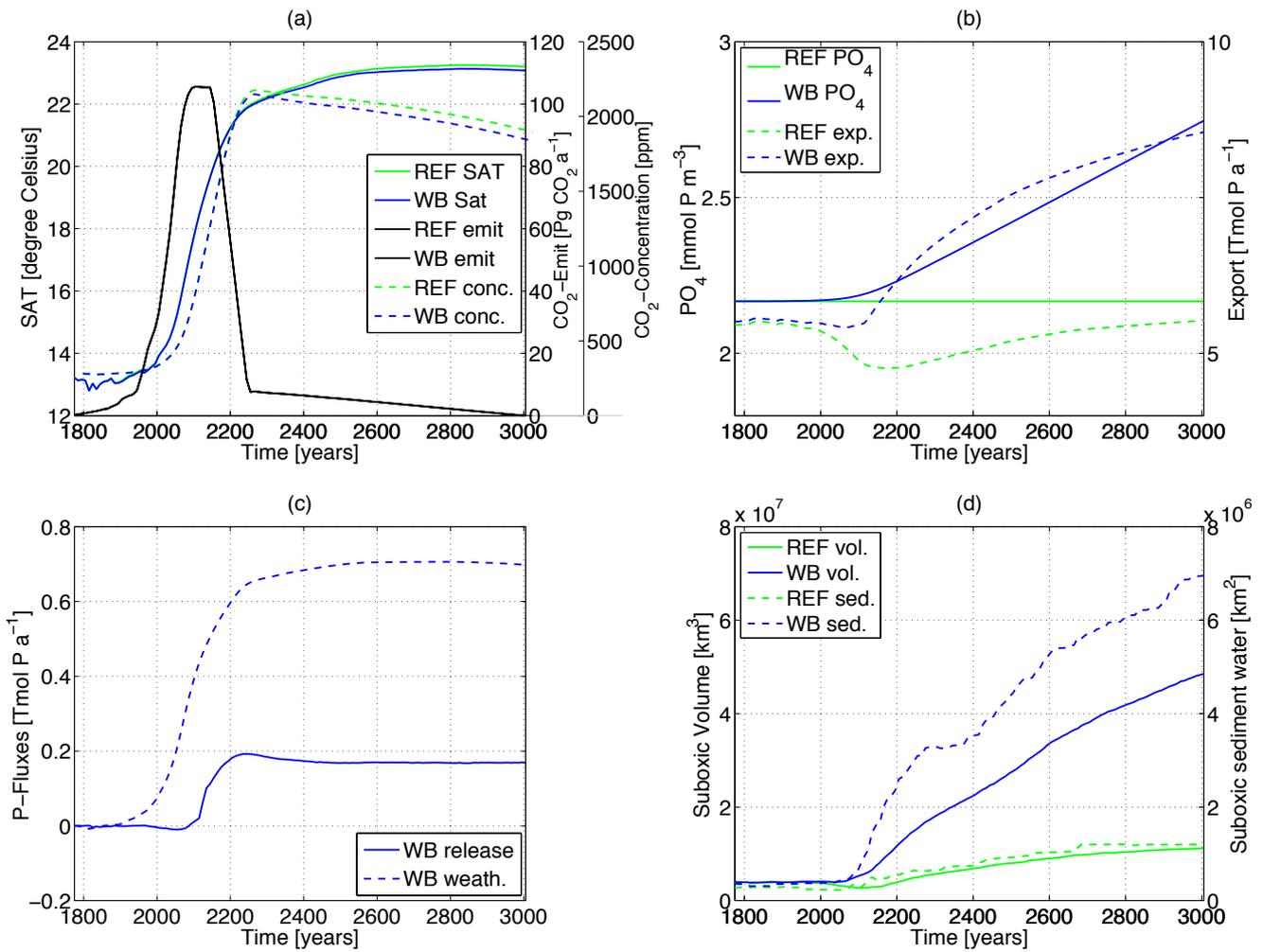
Figure 2: Global and annual mean time series of (a) surface air temperature in degree Celsius (solid lines), CO$_2$-emissions in Pg CO$_2$ a^{-1} (black solid line (for both simulations)) and CO$_2$-concentration in ppm (dashed lines); (b) global mean phosphorus concentration in mmol P m^{-3} (solid lines) and export rate in Tmol P a^{-1} at 130 m depth (dashed lines); (c) anomalies of phosphorus input via sediment in Tmol P a^{-1} (solid line) and anomalies of phosphorus weathering input in Tmol P a^{-1} (dashed line); (d) suboxic volume (<0.005 mol m^{-3}) of the ocean in km^3 (solid lines) and surface of ocean bottom layer with O$_2$ concentrations below 0.005 mol m^{-3} in km^2 (dashed lines). The control simulation (REF) is shown in green, simulation WB in blue.
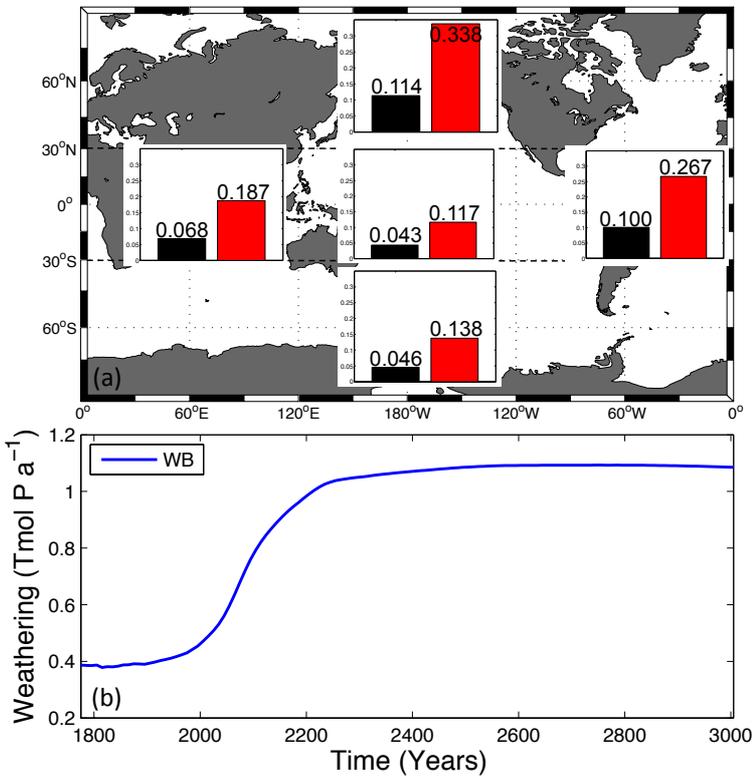
Figure 3: (a) Phosphorus weathering input (in Tmol a⁻¹) into the tropical Pacific Ocean (middle), tropical Atlantic Ocean (right, middle), tropical Indian Ocean (left, middle), Northern Oceans (=oceans north of 30° N; upper middle) and Southern Ocean (=ocean south of 30° S; lower middle) in 1775 (black bars) and 3005 (red bars). (b): Annual mean averaged phosphorus weathering input (global sum) of 1775 until year 3005.
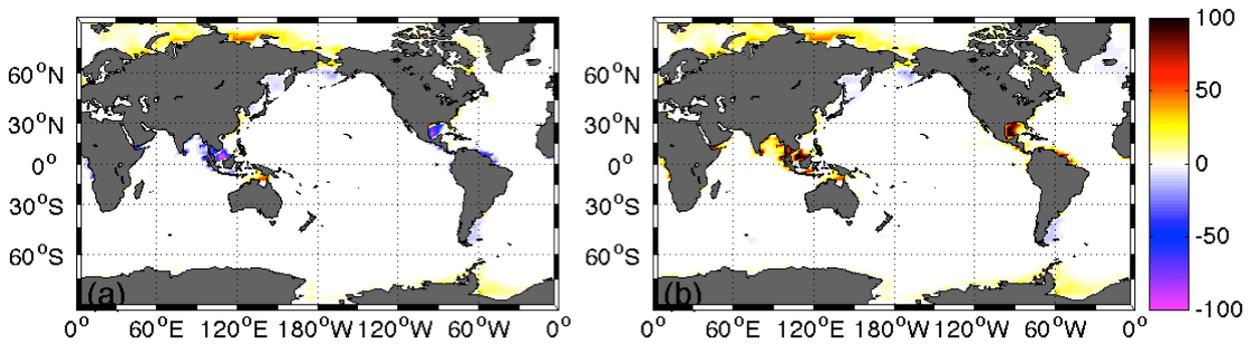
Figure 4: Difference (year 3005 minus year 1775) in (a) burial and (b) benthic release flux in mmol P m⁻² a⁻¹ for simulation WB.
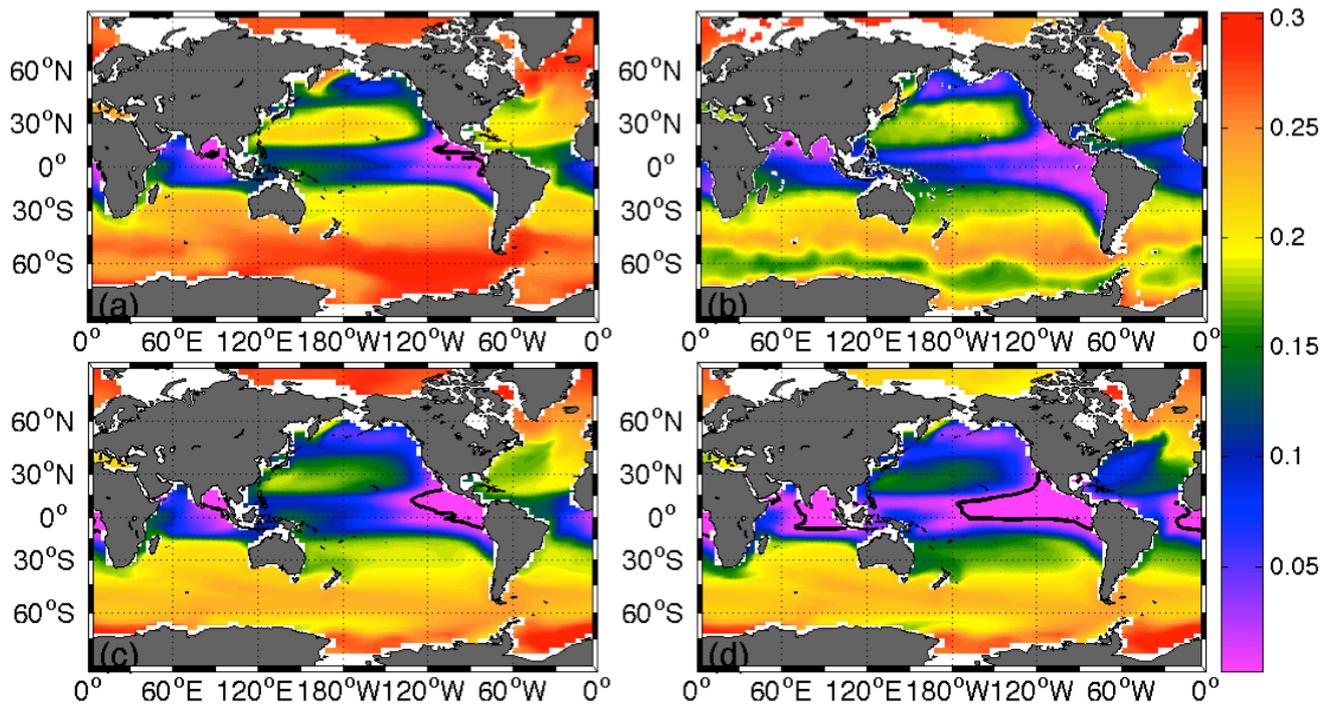
Figure 5: Oxygen concentration in mol O$_2$ m^{-3} at 300m depth simulated by the (a) control simulation at year 1775 (representative for both REF and WB model runs in year 1775), (b) the World Ocean Atlas in 2009, (c) the control simulation at year 3005 and (d) simulation WB at year 3005. The black contour lines at 0.005 mol m^{-3} highlight the oxygen minimum zones (OMZs).